JOURNAL OF THE AMERICAN CHEMICAL SOCIETY

COMMUNICATION

pubs.acs.org/JACS

Controlled Chlorine Plasma Reaction for Noninvasive Graphene Doping

Justin Wu,[†,§] Liming Xie,[†,§] Yanguang Li,[†] Hailiang Wang,[†] Yijian Ouyang,[‡] Jing Guo,[‡] and Hongjie Dai*[,†]

[†]Department of Chemistry, Stanford University, Stanford, California 94305, United States

[‡]Department of Electrical and Computer Engineering, University of Florida, Gainesville, Florida 32611, United States

Supporting Information

ABSTRACT: We investigated the chlorine plasma reaction with graphene and graphene nanoribbons and compared it with the hydrogen and fluorine plasma reactions. Unlike the rapid destruction of graphene by hydrogen and fluorine plasmas, much slower reaction kinetics between the chlorine plasma and graphene were observed, allowing for controlled chlorination. Electrical measurements on graphene sheets, graphene nanoribbons, and large graphene films grown by chemical vapor deposition showed p-type doping accompanied by a conductance increase, suggesting nondestructive doping via chlorination. Ab initio simulations were performed to rationalize the differences in fluorine, hydrogen, and chlorine functionalization of graphene.

To realize the full potential of graphene, an interesting two-dimensional carbon material, various approaches have been used to alter its structures through chemical modification in order to achieve new properties such as band-gap engineering or doping. Chemical functionalization of graphene, whether by hydrogen,[1] fluorine,[2,3] chlorine,[4] or organic groups[5] is one of these approaches. Different approaches and functionalizations have shown myriad outcomes ranging from graphene p-type[6] or n-type[7,8] doping, widening of its band gap to that of an insulator,[2,4] or passivation of edge structures.[9]

In this work, we focused on plasma reactions for graphene chemical modification. We investigated the chlorine plasma reaction with graphene and compared it with the results obtained using fluorine and hydrogen plasmas. Previous works using several functionalization methods, including high-temperature F_2 exposure and hydrogen plasma,[2−4,9] have shown extensive changes and destruction as a result of covalent reactions with graphene. Exposing graphene to a XeF_2 atmosphere has been found to turn graphene into fluorographene, an insulating material with a band gap of 2.9 eV.[2] Similarly, chlorination via a photochemical process altered graphene into an insulator.[4] Graphane, the product of covalent bonding of hydrogen to graphene, is also highly insulating. All of these functionalizations by Cl, F, and H at high coverage have been shown to destroy the network of graphene, rendering the material insulating.[1]

Here we carried out Cl, F, and H plasma reactions with graphene and graphene nanoribbons (GNRs). Raman spectroscopy found that the chlorine plasma reaction with graphene exhibited the slowest kinetics, with the slowest increase of disorder over reaction time (in minutes). In contrast, defects and disorder during plasma fluorination and hydrogenation of graphene increased much more rapidly under short plasma exposures (in seconds). Raman and electrical transport measurements revealed p-doping of graphene upon chlorination. Contrary to fluorine and hydrogen plasma-reacted graphene devices, which rapidly decreased in conductance and became insulating, the conductance of Cl plasma-treated graphene sheets and GNRs could be significantly increased as a result of p-doping without introducing extensive structural damage. The results suggest a novel approach for obtaining transparent graphene films with enhanced conductivity.

Pristine graphene sheets were prepared on SiO_2/Si substrates (oxide thickness of 300 nm) by mechanical exfoliation.[10] Single- and few-layer graphene sheets were identified by optical microscopy and confirmed by Raman spectroscopy.[11] The graphene samples were calcined at 400 °C to remove possible residues before plasma treatment. Micro-Raman spectroscopic mappings of the same graphene sheets were made before and after plasma treatment using a Horiba HR800 Raman system with 532 nm excitation. The plasma treatments were done in an electron cyclotron resonance (ECR) plasma etcher (Astex Plasmaquest model 357) at an ECR power of 200 W and a radiofrequency power of 2 W with 10 mTorr Cl_2, CF_4, or H_2 at room temperature. The power and pressure were held constant over the three plasmas attempted.

Figure 1a−c shows representative Raman spectra of single-layer graphene treated with Cl_2 plasma, CF_4 plasma, and H_2 plasma, respectively. For Cl plasma-treated graphene, the graphitic G band was up-shifted by $\sim$3 cm^{-1} after 30 and 90 s of treatment (Figure 1a), indicating possible p-type doping.[12] The D/G ratio increased only from 0 to 0.3 within 90 s of treatment, indicating that relatively mild disorder and defects (e.g., chlorinated sp^3 carbon sites) were introduced by 90 s of Cl plasma treatment. After 120 s of Cl plasma treatment, the D/G ratio jumped to >2 (Figure 1a,d), indicating that significantly more disorder and defects were generated. On the other hand, H_2 plasma and CF_4 plasma treatments on graphene showed very different results. The most rapid change in D/G ratio of the three plasmas occurred with exposure to hydrogen plasma. A short 10 s exposure of graphene to H_2 plasma led to a D/G ratio of $\sim$3.2. After 30 s of H_2 plasma treatment, no Raman spectrum was detected, and atomic force microscopy (AFM) imaging revealed that the single-layer regions of graphene had been completely etched [see Figure S1a,b in the Supporting Information (SI)].

Received: September 27, 2011
Published: November 14, 2011

 © 2011 American Chemical Society

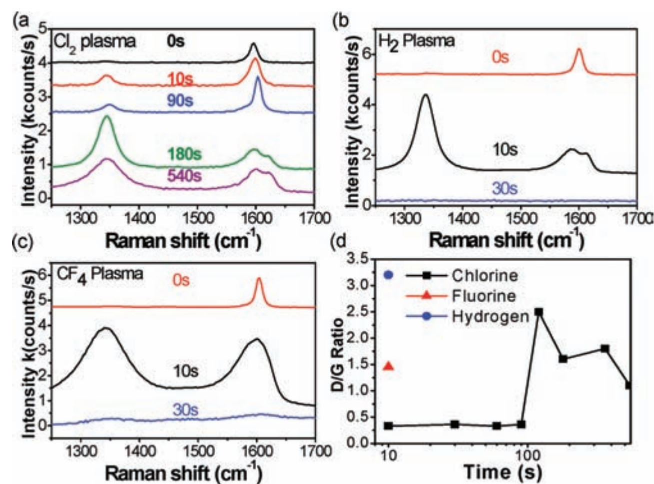

Figure 1. (a−c) Raman spectra of graphene sheets after plasma treatments of varying time using (a) Cl_2, (b) H_2, and (c) CF_4 plasmas. (d) D/G ratio as a function of reaction time for the three plasmas. Pristine graphene showed no D band.

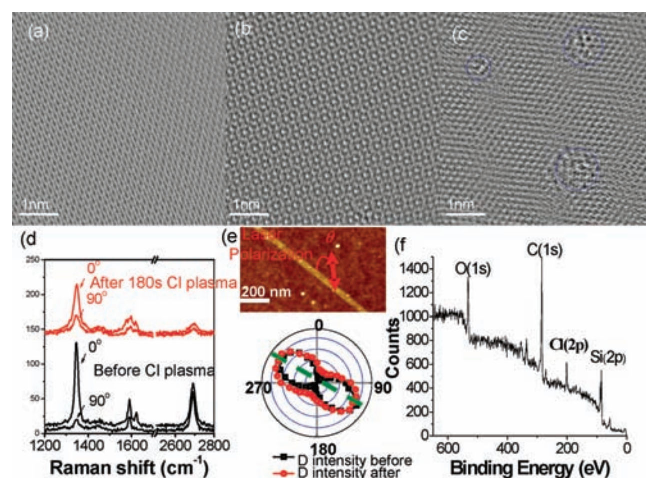

Figure 2. (a−c) TEM images of in-plane regions of (a) an as-made GNR, (b) a GNR treated for 1 min in Cl_2 plasma, and (c) a GNR treated for 180 s in Cl_2 plasma. In (c), areas of introduced defects are circled in blue. (d) Raman spectra of a GNR at parallel and perpendicular polarizations both before and after 3 min of plasma treatment. (e) Lower panel: normalized intensity of the D band as a function of polarization angle before and after plasma treatment. The intensity scale is linear from zero. The olive dashed line indicates the GNR axis direction. Top panel: AFM image of the measured GNR. (f) XPS spectrum of a single sheet of CVD-grown graphene treated for 60 s in Cl_2 plasma. The Si peak was due to the substrate used.

Similarly, Raman spectroscopy of the fluorine plasma-treated sample revealed a rapid D/G ratio increase after 10 s of treatment and disappearance of the D and G peaks after 30 s of exposure, even though AFM imaging revealed that the single-layer film was still physically present in these areas (Figure S1c,d).

Compared with the H and F plasmas, Cl plasma showed the weakest reactivity: the D/G ratio remained ∼0.3 until ∼2 min of reaction, after which the D band increased greatly in intensity in a short period of time (Figure 1d). To probe the defects introduced by the Cl plasma, aberration-corrected atomic-resolution transmission electron microscopy (TEM) imaging was done on GNRs with and without Cl plasma treatment. The GNRs were prepared by sonochemically unzipping multiwalled carbon nanotubes (MWNTs).[13] This method produces primarily bilayer GNRs with several percent single-layer GNRs.[14] The untreated GNRs showed smooth edges and few defects in the plane. The Moiré patterns indicated non-AA/AB stacking of the graphene layers in the GNRs (Figure 2a−c). TEM images of GNRs treated with Cl plasma for 1 min exhibited similar structures without significant disorder (Figure 2b). TEM images of GNRs after 3 min of Cl plasma treatment, in contrast, showed obvious disorder and defects within the plane of the GNRs (Figure 2c), consistent with the Raman data showing that extended Cl plasma treatment (>2 min) introduced appreciable defects in graphene (Figure 1d).

Polarized Raman spectroscopy measurements on individual GNRs were conducted to probe the defects introduced by Cl plasma treatment (Figure 2d,e). Because of the D-band contribution from the GNR edges, the D/G ratio alone is not the sole indicator of GNR quality. The ratio of the D-band intensities at parallel and perpendicular laser polarizations (the $D_{\parallel}/D_{\perp}$ ratio) can be used as an indicator of the GNR quality (edge roughness and defects within the GNR plane).[14,15] An untreated GNR showed a high $D_{\parallel}/D_{\perp}$ ratio of 14 (Figure 2d), indicating smooth edges and few defects.[14−16] The same GNR after 3 min of exposure to Cl plasma exhibited a significantly reduction in the $D_{\parallel}/D_{\perp}$ ratio from 14 to 3.3, indicating a more defective nature as observed by TEM. All of the Raman bands (D, G, 2D) of the GNR showed weaker intensities after 3 min of Cl plasma treatment because of defects introduced to the graphitic structure of the ribbon. Reduced $D_{\parallel}/D_{\perp}$ ratios and D, G, and 2D Raman intensities were also observed for several other GNRs after 3 min of Cl plasma treatment (Figure S2a,b).

A large chemical vapor deposition (CVD)-grown graphene film was subjected to chlorine plasma treatment and subsequent X-ray photoelectron spectroscopy (XPS) measurements (Figure 2f). The graphene film was grown on a Cu film at 950 °C in methane and hydrogen[17] and transferred to a gold substrate. In the transfer process, $Fe(NO_3)_3$ instead of $FeCl_3$ was used to etch Cu in order to avoid chlorine contamination. The sample was then treated with Cl_2 plasma for 60 s; a control film sample without any plasma treatment was also measured. The XPS spectrum revealed a coverage of 8.5 atom % Cl, while the control sample showed no detectable chlorine (Figure 2f and Figure S4a). We used CVD-grown graphene for XPS because it requires a large sample size. The CVD film was likely to have a higher rate of reaction with chlorine plasma than pristine peel-off graphene because of the greater number of defects in the film.[17] This measurement likely does not accurately reflect the quantitative chlorination percentage in pristine graphene on the same time scale but does support the conclusion that chlorine is bonded to the carbon structure.

The Raman data (Figure 1a−d) and TEM images (Figure 2a−c) suggest that there are essentially two stages of the reaction between Cl plasma and graphene. Within ∼90 s of plasma treatment (under the plasma condition used), chlorination of graphene exhibited a much lower reaction rate and was much less destructive than H and F plasmas. Annealing of the graphene samples treated with 1min Cl plasma (within the first stage) in vacuum at 400 °C was found to fully recover the original D/G ratio (Figure S3a−c). This could correspond to the initial stage of Cl attachment to C atoms at defects or other more reactive sites in graphene. The second stage of Cl plasma treatment

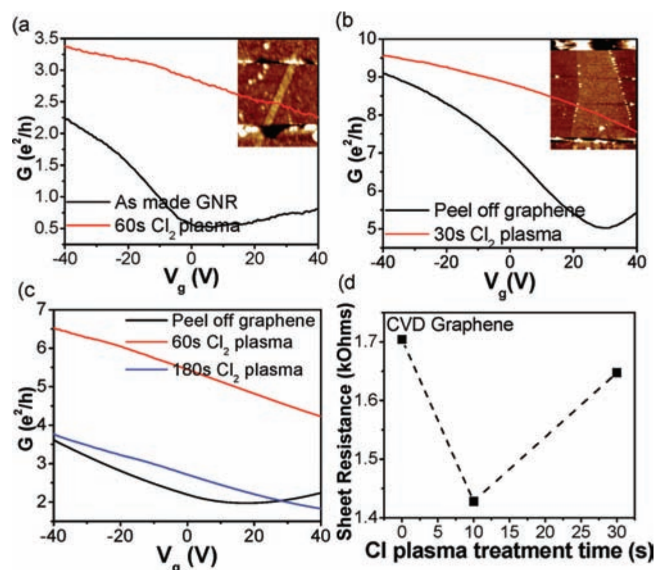

Figure 3. a) $I_{ds}-V_g$ characteristics of a GNR device before and after plasma treatment taken at a source drain bias (V_{ds}) of 1 mV in ambient air. (b) $I_{ds}-V_g$ characteristics of a graphene sheet device before and after treatment, taken at V_{ds} = 1 mV. (c) $I_{ds}-V_g$ characteristics of a graphene sheet device treated for a longer period of time, taken at V_{ds} = 1 mV. (d) Sheet resistance of a single sheet of CVD-grown graphene as a function of time.

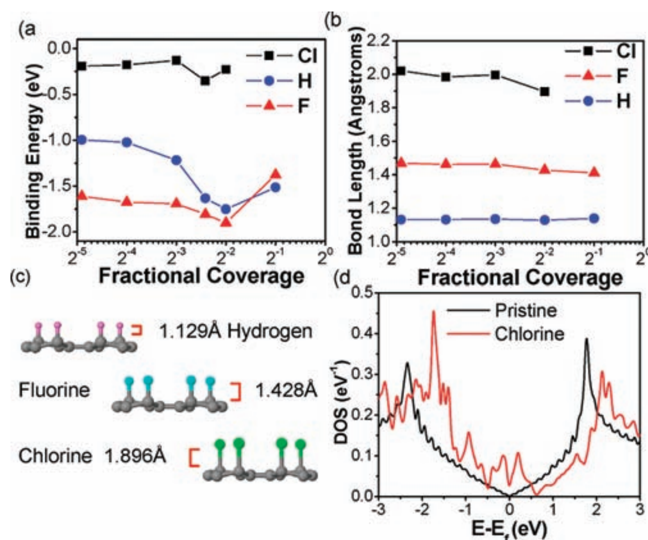

Figure 4. (a) Binding energies and (b) bond lengths of the C−X bond (X = Cl, H, F) as functions of coverage, as calculated by ab initio simulations. (c) Atomistic structures and C−X bond lengths of the different functionalizations of graphene. (d) Calculated DOS of graphene with a $^1/_{30}$ coverage of Cl atoms in comparison with that of pristine graphene as a function of energy $E - E_F$, where E_F is the Fermi energy in each case.

(>120 s) appeared to introduce more defects and could correspond to the expansion of chlorinated regions. This stage was found to be irreversible; while annealing the treated graphene samples reduced the D/G ratio, the result still had substantially more D band than the original pristine graphene (Figure S3d−f). While the detailed reaction pathways remain unclear, these results suggest that the first stage of the Cl plasma reaction, where chlorination occurs without introducing extensive defects, could be controlled and exploited for modifications of graphene and GNRs to afford useful physical properties.

We fabricated graphene devices using pristine peel-off graphene sheets on SiO_2/Si substrates. GNR devices were also made after spin-coating a GNR suspension onto 300 nm SiO_2/Si substrates.[13] The graphene sheets and GNRs were identified and located by AFM imaging and contacted by 18 nm Pd/4 nm Au electrodes defined by e-beam lithography to form source and drain contacts. To improve the contact resistance, the devices were annealed in Ar at 200 °C.[18] The devices were then electrically annealed in a vacuum probe station at 10^{-6} Torr to remove adsorbates until the Dirac points of the drain current-versus-gate voltage ($I_{ds}-V_g$) curves appeared near V_g = 0 V.[7,19] After the devices were electrically annealed to ensure that only the conductance change due to chlorination would be probed (as opposed to the effect of ambient air doping), the devices were carefully measured after re-exposure to ambient air and then placed back into vacuum and measured prior to being subjected to plasma reaction. The devices were exposed to plasma for 60 s and remeasured in ambient air and vacuum to determine the effects of the Cl plasma reaction (Figure 3a).

The maximum conductance (measured at V_g = −40 V) of 1 min Cl plasma-treated GNR devices was found to increase by 1.3−2.2 times the initial conductance in the ambient air (Figure 3a). According to the measured AFM height, these devices were mostly bilayer GNRs.[14] In addition, the devices were found to be significantly p-doped, as none of the devices showed Dirac points within the V_g range after Cl plasma treatment. That is, the Dirac point of the GNR devices had shifted to a high positive V_g outside the accessible range. Peeled-off graphene sheet devices were measured for comparison with the GNR devices (Figure 3b). The results were similar to those for the GNR devices, with the maximum conductance of the graphene sheet devices increased by a factor of 1.04−1.8 relative to the ambient value (contrary to the rapid decrease in conductance for fluorine and hydrogen plasma-reacted graphene devices shown in Figure S4a), with no Dirac point accessible by back-gate voltages. The p-doping was consistent with the observed G-band upshift in the Raman characterization (Figure 1a). Also tested was a plasma reaction time of 180s; the resulting measurements showed a decrease in conductance relative to the original state (Figure 3c).

In view of the possible application of graphene for transparent conductors, we investigated sheet resistance changes of large CVD-grown graphene films resulting from chlorine plasma treatment. The as-grown graphene on a copper substrate was transferred onto a 300 nm SiO_2/Si substrate,[17] and Raman spectroscopy was performed to confirm the single-layer nature of the film over the majority of the area. Four-point van der Pauw measurements were performed to probe the resistance before and after Cl plasma treatment (Figure 3d).[20] It was found that the sheet resistance of the CVD-grown sheets was decreased by a factor of 1.1−1.3 (8−24%) after 10 s of exposure. Longer Cl plasma treatment caused the CVD graphene resistance to increase on a much shorter time scale than for the GNR or peel-off graphene sheet devices. This likely occurred because the defect density and domain edges of CVD graphene make it more reactive, so the sample would be more rapidly affected by the plasma exposure. The obvious increase in conductance for the macroscopic Cl-treated CVD graphene suggests that the conductance increase should be due to doping of the graphene sheet (as reflected in the shift of the Raman peak) instead of a purely contact effect.

Taken together, the electrical data reveal enhanced electrical conductance of peel-off graphene, GNRs, and CVD-grown graphene films resulting from controlled chlorination.

To rationalize the effects of plasma treatment on graphene, *ab initio* simulations (see the SI for details) were performed for Cl, F, and H binding with one side of graphene (as our graphene was deposited on substrates with the bottom side protected) in order to gauge the relative reactivity of each of the plasma species. Both the bond lengths and bond energies were calculated as a function of the fractional coverage (Figure 4a,b). Regardless of the coverage of sp^3 species, we found that the chlorine bond to graphene showed significantly lower binding energy and longer bond length (Figure 4c) than bonds to fluorine or hydrogen. The fact that the simulated chlorine binding energy is significantly smaller than that of hydrogen and fluorine suggests that the reaction is energetically less favorable (Figure 4a), which is consistent with the observation of the low chlorination rate in Figure 1a. In regard to the reactions of hydrogen versus fluorine plasmas, while the calculations suggested that the thermodynamics of the hydrogen reaction is less energetically favorable than the fluorine reaction, the Raman data indicated that the reaction occurs more rapidly. The hydrogen reaction appears to etch the graphene rapidly (Figure S1a,b), as opposed to fluorination, through which the modeled fluorinated structure is the final product. Thus, the energetics from simulations may not fully reflect the entire reaction. It should also be noted that the connection between the binding energy and the reaction rate is only qualitative and can be complicated by sp^3 hybridization and etching defects. Figure 4d compares the calculated density of states (DOS) of pristine graphene and chlorinated graphene at $^1/_{30}$ coverage. After chlorination, the DOS $D(E)$ increases in the energy range $E < 0$, and the Dirac point [the energy at which $D(E) \approx 0$] is ~0.6 eV above the Fermi energy (E_F), indicating p-type doping. Furthermore, Mulliken charge analysis showed that an electron charge of ~0.2 is transferred from graphene to each chlorine atom.

In summary, we have investigated the reactions of chlorine, hydrogen, and fluorine plasmas with several types of graphene materials and found that chlorine plasma is the weakest and most controllable for graphene doping. This is consistent with the weaker binding energy between Cl and graphene as determined by ab initio calculations. Further investigation of chlorine plasma effects on graphene suggests that the length of exposure results in two stages: in the first stage, chlorination occurs fairly nondestructively and reversibly; in the second, at longer exposure times, larger-area defects begin to form irreversibly. In the shorter time frame, XPS directly showed the presence of chlorine. Exfoliated graphene and GNR devices showed p-type doping, and four-point measurements on CVD-grown graphene showed an increase in conductance.

ASSOCIATED CONTENT

Supporting Information. Experimental procedures, GNR and CVD growth of graphene, TEM and Raman characterization, device fabrication, details regarding the binding energy calculations, AFM images after hydrogen or fluorine plasma treatment, additional Raman spectra of GNRs, Raman spectra showing the reversibility of chlorination, XPS of the control sample, and conductivity measurements on a fluorinated device. This material is available free of charge via the Internet at http://pubs.acs.org.

AUTHOR INFORMATION

Corresponding Author
hdai1@stanford.edu

Author Contributions
[§]These authors contributed equally.

ACKNOWLEDGMENT

This work was supported by MARCO MSD, Intel, ONR MURI on graphene, and Samsung Electronics. The work at UF was supported by ONR and NSF. TEM was done at the National Center for Electron Microscopy at Lawrence Berkeley National Laboratory, which is supported by the U.S. Department of Energy under Contract DE-AC02-05CH11231.

REFERENCES

(1) Elias, D. C.; Nair, R. R.; Mohiuddin, T. M. G.; Morozov, S. V.; Blake, P.; Halsall, M. P.; Ferrari, A. C.; Boukhvalov, D. W.; Katsnelson, M. I.; Geim, A. K.; Novoselov, K. S. *Science* **2009**, *323*, 610.

(2) Robinson, J. T.; Burgess, J. S.; Junkermeier, C. E.; Badescu, S. C.; Reinecke, T. L.; Perkins, F. K.; Zalalutdniov, M. K.; Baldwin, J. W.; Culbertson, J. C.; Sheehan, P. E.; Snow, E. S. *Nano Lett.* **2010**, *10*, 3001.

(3) Withers, F.; Dubois, M.; Savchenko, A. K. *Phys. Rev. B* **2010**, *82*, No. 073403.

(4) Li, B.; Zhou, L.; Wu, D.; Peng, H.; Yan, K.; Zhou, Y.; Liu, Z. *ACS Nano* **2011**, *5*, 5957.

(5) Farmer, D. B.; Lin, Y.; Afzali-Ardakani, A.; Avouris, P. *Appl. Phys. Lett.* **2009**, *94*, No. 213106.

(6) Chen, W.; Chen, S.; Qi, D. C.; Gao, X. Y.; Wee, A. T. S. *J. Am. Chem. Soc.* **2007**, *129*, 10418.

(7) Wang, X.; Li, X.; Zhang, L.; Yoon, Y.; Weber, P. K.; Wang, H.; Guo, J.; Dai, H. *Science* **2009**, *324*, 768.

(8) Lin, Y.; Lin, C.; Chiu, P. *Appl. Phys. Lett.* **2010**, *96*, No. 133110.

(9) Lu, Y. H.; Wu, R. Q.; Shen, L.; Yang, M.; Sha, Z. D.; Cai, Y. Q.; He, P. M.; Feng, Y. P. *Appl. Phys. Lett.* **2009**, *94*, No. 122111.

(10) Novoselov, K. S.; Geim, A. K.; Morozov, S. V.; Jiang, D.; Zhang, Y.; Dubonos, S. V.; Grigorieva, I. V.; Firsov, A. A. *Science* **2004**, *306*, 666.

(11) Malard, L. M.; Pimenta, M. A.; Dresselhaus, G.; Dresselhaus, M. S. *Phys. Rep.* **2009**, *473*, 51.

(12) Subrahmanyam, K. S.; Voggu, R.; Govindaraj, A.; Rao, C. N. R. *Chem. Phys. Lett.* **2009**, *472*, 96.

(13) Jiao, L.; Wang, X.; Diankov, G.; Wang, H.; Dai, H. *Nat. Nanotechnol.* **2010**, *5*, 321.

(14) Xie, L.; Wang, H.; Jin, C.; Wang, X.; Jiao, L.; Suenaga, K.; Dai, H. *J. Am. Chem. Soc.* **2011**, *133*, 10394.

(15) Casiraghi, C.; Hartschuh, A.; Qian, H.; Piscanec, S.; Georgi, C.; Fasoli, A.; Novoselov, K. S.; Basko, D. M.; Ferrari, A. C. *Nano Lett.* **2009**, *9*, 1433.

(16) Cançado, L. G.; Pimenta, M. A.; Neves, B. R. A.; Dantas, M. S. S.; Jorio, A. *Phys. Rev. Lett.* **2004**, *93*, No. 247401.

(17) Li, X.; Cai, W.; An, J.; Kim, S.; Nah, J.; Yang, D.; Piner, R.; Velamakanni, A.; Jung, I.; Tutuc, E.; Banerjee, S. K.; Colombo, L.; Ruoff, R. S. *Science* **2009**, *324*, 1312.

(18) Javey, A.; Guo, J.; Wang, Q.; Lundstrom, M.; Dai, H. *Nature* **2003**, *424*, 654.

(19) Moser, J.; Barreiro, A.; Bachtold, A. *Appl. Phys. Lett.* **2007**, *91*, No. 163513.

(20) Van der Pauw, L. J. *Philips Res. Rep.* **1958**, *13*, 1.